Biochemical Pharmacology 80 (2010) 226–235

Contents lists available at ScienceDirect

Biochemical Pharmacology

journal homepage: www.elsevier.com/locate/biochempharm

Photodynamic therapy targeting neuropilin-1: Interest of pseudopeptides with improved stability properties

Noémie Thomas [a], Marlène Pernot [a], Régis Vanderesse [b,f], Philippe Becuwe [c], Ezatul Kamarulzaman [b], David Da Silva [d], Aurélie François [a], Céline Frochot [e,f], François Guillemin [a,f], Muriel Barberi-Heyob [a,f,*]

[a] Centre de Recherche en Automatique de Nancy (CRAN), Nancy-University, CNRS, Centre Alexis Vautrin, Vandœuvre-lès-Nancy, France
[b] Laboratoire de Chimie Physique Macromoléculaire (LCPM), Nancy-University, CNRS, Nancy, France
[c] EA 4421 SIGReTO, Nancy-University, Vandœuvre-lès-Nancy, France
[d] Laboratoire de Spectrométrie de Masse et de Chimie Laser, Institut Jean Barriol - Fédération de Recherche 2843, Paul Verlaine-University, Metz, France
[e] Laboratoire Réactions et Génie des Procédés (LRGP), Nancy-University, CNRS, Nancy, France
[f] GDR CNRS 3049 "Médicaments Photoactivables - Photochimiothérapie (PHOTOMED)", France

ARTICLE INFO

Article history:
Received 29 January 2010
Accepted 31 March 2010

Keywords:
Targeted photodynamic therapy
Pseudopeptide
Neuropilin-1
siRNA
Affinity
In vivo stability

ABSTRACT

The general strategy developed aims to favor the vascular effect of photodynamic therapy by targeting tumor vasculature. Since angiogenic endothelial cells represent an interesting target to potentiate this vascular effect, we previously described the conjugation of a photosensitizer to a peptide targeting neuropilins (NRPs) over-expressed specially in tumor angiogenic vessels and we recently characterized the mechanism of photosensitization-induced thrombogenic events. Nevertheless, in glioma-bearing nude mice, we demonstrated that the peptide moiety was degraded to various rates according to time after intravenous administration. In this study, new peptidases-resistant pseudopeptides were tested, demonstrating a molecular affinity for NRP-1 and NRP-2 recombinant chimeric proteins and devoid of affinity for VEGF receptor type 1 (Flt-1). To argue the involvement of NRP-1, MDA-MB-231 breast cancer cells were used, strongly over-expressing NRP-1 receptor. We evidenced a statistically significant decrease of the different peptides-conjugated photosensitizers uptake after RNA interference-mediated silencing of NRP-1. Peptides-conjugated photosensitizers allowed a selective accumulation into cells. In mice, no degradation was observed in plasma *in vivo* 4 h after intravenous injection by MALDI-TOF mass spectrometry. This study draws attention to this potential problem with peptides, especially in the case of targeting strategies, and provides useful information for the future design of more stable molecules.

1. Introduction

The selectivity of photodynamic therapy (PDT) as an anti-cancer treatment relies on the local generation of cytotoxic reactive oxygen species in the tumor tissue, due to both preferential uptake of the photosensitizer by malignant tissue and subsequent localized light irradiation. Indeed, the photosensitizer, at the concentrations used for PDT, is non-toxic in the dark and becomes photocytotoxic only when light at an appropriate wavelength is applied. However, the tumor tissue selectivity remains limited, as photosensitizers also tend to accumulate in normal tissue. This selectivity can be improved by using third generation photosensitizers, which consist of photosensitizers to which a tumor-targeting moiety is attached [1]. Among the tumor-targeting molecules, peptides are receiving increasing interest in the field of PDT. Indeed, the effective tissue penetration of short synthetic peptides, in combination with their selective binding and internalizing capacity by cancer cells, make peptides ideal candidates for the delivery of therapeutic agents such as photosensitizers [2].

Abbreviations: AcOH, acetic acid; Ahx, 6-aminohexanoic acid; a.u., arbitrary units; a.i., arbitrary intensity; CHAPS, 3-[(3-cholamidopropyl)dimethylammonio]-1-propanesulfonate; DCC, dicyclohexylcarbodiimide; DIEA, *N,N*-diisopropylethylamine; a.i., arbitrary intensity; DMF, dimethylformamide; DLI, drug-light interval; EDTA, ethylene diamine tetra acetic acid; FBS, fetal bovine serum; Flt-1, fms-like tyrosine kinase 1; Fmoc, 9-fluorenyl-methoxy-carbonyl; HOBt, 1-hydroxybenzotriazole; HPLC, high performance liquid chromatography; HUVEC, human umbilical vein endothelial cells; i.v., intravenous; MALDI-TOF, matrix assisted laser desorption ionisation-time-of-flight; $NaBH_3CN$, sodium cyanoborohydride; NHS, *N*-hydroxysuccinimide; NRP, neuropilin; NRP-1, neuropilin-1; NRP-2, neuropilin-2; PDT, photodynamic therapy; PEG, polyethylene glycol; PMSF, phenylmethylsulphonyl fluoride; RER, relative expression ratio; RNAi, RNA interference; RP-HPLC, reverse phase-high performance liquid chromatography; RT-PCR, reverse transcription-polymerase chain reaction; s.d., standard deviation; siRNA, small interfering RNA; tBu, tertio-butyl; TBTU, 2-(1*H*-benzotriazol-1-yl)-1,1,3,3-tetramethyl-uronium tetrafluoroborate; TFA, trifluoroacetic acid; TIS, triethylsilane; TLC, thin layer chromatography; TPC, 5-(4-carboxyphenyl)-10,15,20-triphenylchlorin; VEGF, vascular endothelial growth factor; Wt, wild type.

* Corresponding author at: Centre de Recherche en Automatique de Nancy, Centre Alexis Vautrin, Avenue de Bourgogne, Brabois, F-54511 Vandœuvre-lès-Nancy, France. Tel.: +33 3 83 59 83 76.
E-mail address: m.barberi@nancy.fnclcc.fr (M. Barberi-Heyob).

0006-2952/$ – see front matter © 2010 Elsevier Inc. All rights reserved.
doi:10.1016/j.bcp.2010.03.036

Destruction of the neovasculature of tumors by PDT is thought to play a major part in the destruction of some vascularized tumors [3–5]. In order to potentiate the vascular effect of PDT, receptors specifically located on angiogenic endothelial cells, such as receptors to vascular endothelial growth factor (VEGF), can be used as molecular targets. We have previously described the conjugation of a photosensitizer (5-(4-carboxyphenyl)-10,15,20-triphenyl-chlorin, TPC), *via* a spacer (6-aminohexanoic acid, Ahx), to a heptapeptide (ATWLPPR), specific for the VEGF receptor neuropilin-1 (NRP-1), and reported the *in vitro* and *in vivo* efficacy of this new peptide-conjugated photosensitizer (referred to hereafter as TPC-Ahx-ATWLPPR) [6,7].

Despite their advantages as targeting agents, the main disadvantage of peptides is related to their structural conformation which makes them extremely sensitive to peptidases [8]. They often display low stability in biological fluids, which limits their use *in vivo*. Photosensitizer moiety of TPC-Ahx-ATWLPPR is responsible for the photocytotoxic activity of the conjugate, while the peptidic part is responsible for its selectivity. Degradation of the peptidic moiety of the conjugate would impair its selectivity, and would both allow it to accumulate in normal tissues, where the activated photosensitizer could exert non-desirable photocytotoxicity, and decrease the amount of photosensitizer delivered to targeted tumor tissues. We previously examined the *in vivo* stability of TPC-Ahx-ATWLPPR by high performance liquid chromatography (HPLC) and matrix assisted laser desorption ionisation-time-of-flight (MALDI-TOF) mass spectrometry. TPC-Ahx-ATWLPPR was stable *in vitro* in plasma but, following intravenous injection (i.v.) in nude mice, was degraded to various rates and TPC-Ahx-A was identified as the main metabolic product [9,10]. The use of peptidases-resistant pseudopeptides would increase further its stability *in vivo* without loss of affinity [11–13]. We identified the major site of degradation between A and T amino acids, leading us to suggest the synthesis of two modified peptides (aTWLPPR where a is (*R*)Ala, Aψ[CH_2NH]TWLPPR, where the amide bond between A and T residues is replaced by a –CH_2NH– bond, Fig. 1A). In the current study, we validate the chemical identity and the photophysical characteristics of these new conjugates and propose to demonstrate by competitive binding experiments that these pseudopeptides and conjugates describe an affinity for NRPs. Taking advantage of RNA silencing techniques known as RNA interference (RNAi), we have selectively silenced NRP-1 expression in MDA-MB-231 breast cancer cells to provide the evidence for the involvement of NRP-1 expression in conjugated photosensitizer cellular uptake. We also studied *in vivo* stability of the conjugated pseudopeptides by MALDI-TOF mass spectrometry.

2. Materials and methods

2.1. Synthesis of ATWLPPR, aTWLPPR and Aψ[CH_2NH]TWLPPR and purification

Unless otherwise stated, reagents were purchased from chemical companies and used without prior purification. Reagent grade solvents were used as received. 5-(4-carboxyphenyl)-10,15,20-triphenyl-chlorin (TPC) was purchased from Porphyrin Systems (Lübeck, Germany). Fmoc-Arg(Pbf)-Wang, Fmoc-aminoacids, and Fmoc-aminohexanoic acid were from Senn Chemicals International (Dielsdorf, Switzerland) or Merck Novabiochem (Laüfelfingen Switzerland). Thin-layer chromatography (TLC) was carried out on Merck silica gel 60 F254 plates (Merck Chimie S.A.S., Fontenay Sous Bois, France) and developed with the appropriate solvents. The TLC spots were visualized either by UV light or by heating plates sprayed with a solution of phosphomolybdic acid (5% ethanolic solution). Chromatography column was carried out on Merck silica gel (40–63 μm; 230–400 mesh ASTM). ATWLPPR, aTWLPPR and Aψ[CH_2NH]TWLPPR were synthesized on a multichannel peptide synthesizer [14], or a fully automated ResPepXL synthesizer (INTAVIS AG, Köln, Germany) according to a classical Fmoc/tBu solid-phase methodology. The side chains of arginine, tryptophan, and threonine were respectively protected by Pbf, Boc and tBu groups. The linker was introduced like an amino acid with Fmoc-Ahx-OH. Double coupling was performed using a 3-fold excess of *N*-Fmoc-amino acid (except during the photosensitizer coupling stage: 2-fold excess and single coupling) and activation reagents 2-(1*H*-benzotriazol-1-yl)-1,1,3,3-tetramethyl-uronium tetrafluoroborate (TBTU) (3 equiv.), 1-hydroxybenzotriazole (HOBt) (3 equiv.) and *N*,*N*-diisopropylethylamine (DIEA) (9 equiv.) in dimethylformamide (DMF). The reduced peptide was synthesized by condensation of 3 equiv. Fmoc-Leu-H, previously described in [15] on the *N*-terminus of growing peptide in DMF in the presence of 3 equiv. $NaBH_3CN$ and some drops of AcOH overnight. The cleavage was realized by a 2 h treatment with TFA/H_2O/TIS (92.5:2.5:5) mixture. Peptides were purified by reverse phase high performance liquid chromatography (RP-HPLC) on a C18 preparative column (150 × 21.2 mm, Pursuit Varian) using a 0.1% (v/v) TFA–water/acetonitrile gradient, monitored by absorbance at 280 nm on a SPD-10A UV–visible detector (Shimadzu, France). Both compounds were lyophilized and kept in aliquots at −20 °C.

2.2. Synthesis of peptides-conjugated chlorin-type photosensitizer and purification

TPC was coupled to the *N*-terminus of the Ahx on the resin via its NHS ester. TPC-NHS was prepared in the dark under a nitrogen atmosphere by action of *N*-hydroxysuccinimide (1 equiv.) and dicyclohexylcarbodiimide (DCC) (1 equiv.) on TPC (1 equiv.) in CH_2Cl_2 for 4 h at room temperature. The solvent was evaporated and the crude material was purified by column chromatography using EtOH/CH_2Cl_2: 4/96 (v/v) as the eluent. The fractions were tested by TLC and the pure compound was isolated as a purple solid (73%). During the photosensitizer coupling stage, light exposure was minimized by sealing the reaction vessel in aluminum foil to limit the occurrence of unwanted side reactions. A standard cleavage with trifluoroacetic acid (TFA) and scavengers afforded the crude peptides-conjugated photosensitizers. Purification was made by reverse phase-high performance liquid chromatography (RP-HPLC) on a C18 semi-preparative column (250 × 10 mm I.D., Apollo, Alltech, Lokeren, Belgium) using a 0.1% (v/v) TFA–water/methanol gradient, monitored by absorbance at 280 nm on a SPD-10A UV–visible detector (Shimadzu, France). Both compounds were lyophilized and kept in the dark in aliquots at −20 °C.

2.3. Chemical characterization. MALDI-TOF mass spectrometry analysis

Five microliters of a 2,5-dihydroxybenzoic acid solution (150 mg/ml in water/acetonitrile, 1:1, v/v) was mixed with 1 μl of sample and spotted on the stainless steel MALDI targets. The solvent was evaporated before insertion in the source. Analyses were performed on a Bruker Reflex IV time-of-flight mass spectrometer (Bruker-Daltonic, Bremen, Germany) equipped with the SCOUT 384 probe ion source. The system used a pulsed nitrogen laser (337 nm, model VSL-337ND, Laser Science Inc., Boston, MA) with a maximal energy of 400 μJ/pulse. Positive ion spectra were acquired with an acceleration voltage of 20 kV and reflector voltage of 23 kV in the 0–2000 Da m/z range. The detector signals were amplified and transferred to the Flex Control software 3.0 (Bruker-Daltonic). Spectra were processed with the Flex Analysis software 3.0 (Bruker-Daltonic). External calibration of

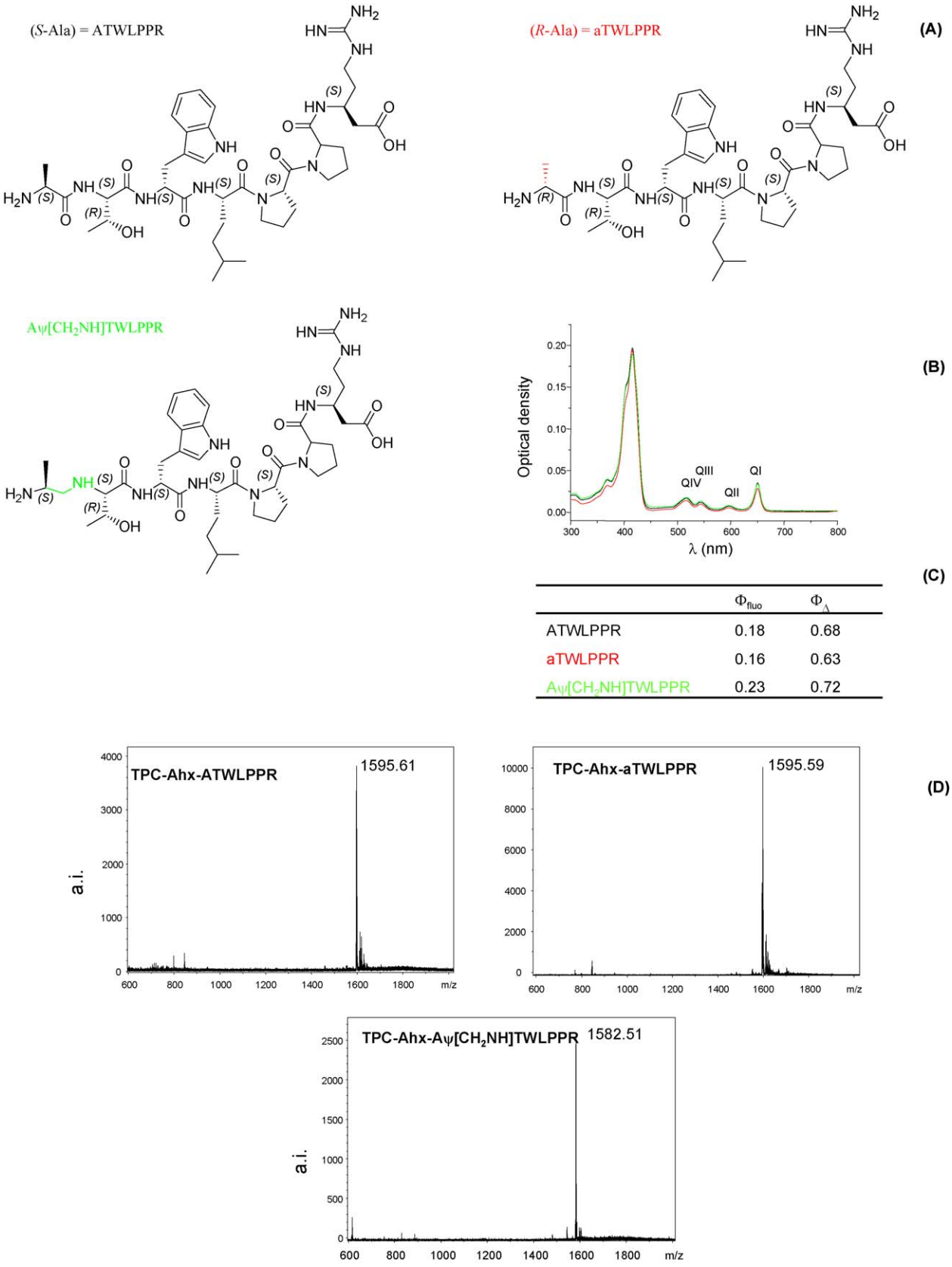

	Φ_{fluo}	Φ_{Δ}
ATWLPPR	0.18	0.68
aTWLPPR	0.16	0.63
Aψ[CH_2NH]TWLPPR	0.23	0.72

Fig. 1. Chemical structures of the peptides and photophysical characteristics of the conjugates. Chemical structures of the heptapeptide (ATWLPPR) and new pseudopeptides (aTWLPPR and Aψ[CH_2NH]TWLPPR) (A). Absorption spectra of TPC-Ahx-ATWLPPR (black), TPC-Ahx-aTWLPPR (red) and TPC-Ahx-Aψ[CH_2NH]TWLPPR (green) in ethanol (B). Fluorescence quantum yields (Φ_{fluo}) and singlet oxygen quantum yields (Φ_{Δ}) of these three peptides-conjugated photosensitizers (C). MALDI-TOF MS spectrum of TPC-Ahx-ATWLPPR, TPC-Ahx-aTWLPPR and TPC-Ahx-Aψ[CH_2NH]TWLPPR (D). (For interpretation of the references to color in this figure legend, the reader is referred to the web version of the article.)

MALDI mass spectra was carried out using sodic and potassic distribution of PEG 600 and PEG 1500 mixtures.

2.4. Photophysical properties

Absorption spectra were recorded on a Perkin-Elmer UV–visible spectrophotometer (Lambda 2, Courtaboeuf, France). Fluorescence spectra were recorded on a SPEX Fluorolog-3 spectrofluorimeter (Jobin Yvon, Longjumeau, France), equipped with a thermostated cell compartment (25 °C), using a 450 W Xenon lamp. The fluorescence quantum yields (Φ_f) in ethanol and quantum yields of singlet oxygen production ($\Phi(^1O_2)$) were determined as described previously [16].

2.5. Binding of peptides and peptides-conjugated TPC to recombinant NRP-1, NRP-2 and Flt-1 proteins

NRP-1, NRP-2 and Flt-1 were obtained from R&D Systems (Lille, France), as recombinant chimeric proteins. The surface of Maxisorp microplates (Dutscher) was coated with either NRP-1 (2 μg/mL), NRP-2 (5 μg/mL) or Flt-1 (2 μg/mL) in PBS, overnight at room temperature. The plates were blocked with PBS containing 0.5% bovine serum albumin (blocking buffer) during 1 h at 37 °C, to prevent non-specific interactions. Binding of the photosensitizer to NRP-1 was assessed using 5 ng/mL of biotinylated $VEGF_{165}$ (R&D Systems) in blocking buffer containing 2 μg/mL heparin. Biotinylated $VEGF_{165}$ was added to the coated wells, in competition, or not, with an excess of peptides-conjugated TPC or TPC or unlabelled $VEGF_{165}$ (R&D Systems), as a positive control. In the case of photosensitizers, 0.5% Tween-20 was added to the blocking buffer in order to allow for its solubilization. After a 2-h incubation at room temperature, the plates were washed and the amount of bound biotinylated $VEGF_{165}$ stained with streptavidin horseradish peroxidase conjugate (R&D Systems) and assayed. After 20 min at room temperature, reaction was stopped by the addition of Stop Solution (R&D Systems). Optical densities were measured at 450 nm. Results were expressed as relative absorbance to wells containing only blocking buffer. Three wells per condition were used.

2.6. Cell lines and culture

For *in vitro* experiments, MDA-MB-231 human breast cancer cells were purchased from American Type Culture Collection (ATCC, Manassas, VA, USA). Cells were maintained in minimum essential medium supplemented with 10% fetal bovine serum (FBS), 1% antibiotic/antimitotic solution. They were cultured in 75 cm^2 flasks and incubated in 5% CO_2/95% humidified air at 37 °C. Cell culture materials were purchased from Costar (Dutscher, Brumath, France). All other chemicals were purchased from Sigma (Saint Quentin Fallavier, France), unless otherwise stated.

2.7. NRP-1-siRNA vector and stable transfection

RNA silencing technique known as RNA interference (RNAi) was used. Small interfering RNA (siRNA) oligonucleotides were obtained from Eurogentec in a purified and annealed duplex form. The sequences targeting the human NRP-1 gene are: 5′-GAGAGGTCCTGAATGTTCC-3′ (sense) and 5′-GGAACATTCAG-GACCTCTCC-3′ (antisense). Scrambled siRNA with the following sequence: 5′-UUAAACUUCAGCCCAGUGA-3′ (sense) and 5′-CAGUAAACGCCGUCUUAUA-3′ (antisense) was used as the control. SiRNA transfection experiments were carried out using jetSi-ENDO transfection reagent with 100 nM siRNA, according to the manufacturer's instructions (Eurogentec). Double strand DNA oligonucleotide encoding the effective siRNA in the knockdown of NRP-1 was synthesized with a loop sequence TTCAAGAGA and a RNA pol III terminator sequence consisting of a 6 poly T. This double strand DNA oligonucleotide was cloned into the RNAi-ready pSIREN vector (BD Biosciences Clontech) between the BamHI and EcoRI restriction sites with the U6 promoter. This vector contains a puromycin resistance gene for the selection of stable transfectants. A unique XbaI restriction site was placed downstream of the terminator sequence for restriction digest analysis to confirm the presence of the cloned insert. Four micrograms of pSIREN/U6/NRP-1-siRNA vector, or pSIREN/U6/scrambled-siRNA vector or pSIREN/U6 empty vector were used for stable transfection of MDA-MB-231 cells with TransPEI transfection reagent, according to the manufacturer's instructions (Eurogentec). The MDA-MB-231 clones were selected with 0.5 μg/mL of puromycin for 3 weeks. Single colonies were isolated and then screened for levels of the expression of NRP-1 protein by reverse transcription-polymerase chain reaction (RT-PCR) and Western blot analyses. Five days before the experiments, the cells were placed into complete medium without puromycin supplement.

2.8. Proteins extraction and immunoblotting

Cells (MDA-MB-231 clones) were collected by scraping, washed with ice-cold phosphate buffered saline (PBS) and treated with lysis buffer, containing 10 mM Tris–HCl (pH 7.4), 1% CHAPS (3-[(3-cholamidopropyl)dimethylammonio]-1-propanesulfonate), 2 mM ethylene diamine tetraacetic acid (EDTA) and 1 mM phenylmethylsulphonyl fluoride (PMSF) for 30 min on ice, and further centrifuged at 15,000 × *g* for 20 min at 4 °C. Total protein concentration was determined using the DC Protein Assay (Bio-Rad, Marnes-la Coquette, France), according to the manufacturer's instructions. Protein samples (25 μg) were heated to 95 °C for 7 min in the presence of 5% 2-mercaptoethanol, chilled on ice and separated on a 7.5% denaturing polyacrylamide gel, followed by electrophoretic transfer to polyvinylidene difluoride membranes. Membranes were blocked with 5% (w/v) non-fat dry milk in Tris-buffered saline containing 0.1% (v/v) Tween-20 (TBST), overnight at 4 °C. Membranes were then incubated for 1 h with polyclonal anti-NRP-1 (sc-7239, Santa Cruz Biotechnology, Tebu, Le Perray en Yvelines, France), diluted 1: 200 in 5% (w/v) non-fat dry milk in TBST. After several washes, the blots were incubated with secondary anti-goat antibody linked to horseradish peroxidase (Donkey Anti-goat IgG,-HRP sc-2020, Santa Cruz, 1:2000). Bound antibody was detected using the ECL detection system (Amersham Biosciences, Orsay, France) and visualized by autoradiography. To ensure equal loading of proteins, blots were subsequently stripped and probed with a polyclonal anti-tubulin (sc-9104, Santa Cruz Biotechnology), using the procedure described above.

2.9. RNA isolation and RT-PCR analysis

Isolation of total RNA was performed using TRIzol Reagent (Invitrogen). cDNA synthesis was perfomed with 1 μg of total RNA in a reaction volume of 20 μL containing 4 μL of BioRad reaction mixture 5× and 1 μL of BioRad Iscript reverse transcriptase (Iscript cDNA synthesis kit BioRad) and incubated 5 min at 25 °C, 30 min at 45 °C and 5 min at 75 °C in a thermocycler eppendorf. Each sample was then stored at −20 °C.

PCR reaction were performed with 2 μL of the reaction cDNA mixture in a volume of 20 μL containing 50 μM of each 5′- and 3′-primers, 1.6 μL dNTP 2.5 nM (Kit In vitrogen dNTP Set), 2 μL Buffer 10×, 0.6 μL $MgCl_2$ 50 mM and finally 0.2 μL of Taq DNA polymerase (Kit In vitrogen TaqDNA pol). The primer sequences were as follows: NRP-1, 5′-ATGGAGAGGGGGCTGCCG-3′ (sense), 5′-CTA TCG CGC TGT CGG TGT A-3′ (antisense) [6]; GAPDH, 5′-TGGGGAAGGT-GAAGGTCGGA-3′ (sense) and 5′-GGATCTCGCTGCTGGAAGA-3′ (an-

tisense) [17]. Tubes were incubated for amplification for 15 min at 95 °C, 1 min at 55 °C and 1 min at 72 °C for cycle 1 (Thermocycler Eppendorf). For Cycle 2-29: 30 s at 95 °C, 1 min at 55 °C and 1 min at 72 °C. For cycle 30: 30 s at 95 °C, 1 min at 55 °C and 10 min at 72 °C. GAPDH and NRP-1 products were analyzed using 1% agarose gel electrophoresis with 1 μg mL^{-1} ethidium bromide. Quantifications were performed by UV transillumination using Gel Doc EQ (BioRad).

2.10. Photosensitizers cellular uptake and selectivity

Cells were seeded in 96 wells plate (2×10^4 cells/well). Two plates per cell line were prepared. After 3 days, medium containing TPC or peptides-conjugated photosensitizers (5 μM) was added for different times, ranging from 2 to 24 h. We previously evaluated the *in vitro* dark cytotoxicity of TPC and TPC-Ahx-ATWLPPR for concentrations ranging from 0.05 to 50 μM and demonstrated that in the absence of light exposure with either photoactive compound yielded a surviving cell fraction higher than 85% for concentrations up to 5.00 μM [7]. Two plates per cell line were used, the first one to evaluate cellular viability using a 3-(4,5-dimethylthiazol-2-yl)-2,5-diphenyl tetrazolium bromide (MTT) assay, the second plate for intracellular incorporation. For photosensitizers cellular uptake, the plate was centrifuged ($1200 \times g$; 5 min), medium was then removed and cells were re-suspended in ethanol. Photosensitizers were extracted by a 10 min-sonication (Branson 1200, Roucaire Instruments Scientifiques, Les Ulis, France). Cell debris were removed by centrifugation ($3500 \times g$; 15 min). Fluorescence (recorded at 652 nm following excitation at 415 nm) was measured on a flx-Xenius spectrofluorimeter (SAFAS, Monaco).

The intracellular uptake of TPC and peptides-conjugated TPC by MDA-MB-231 was visualized by fluorescence microscopy. Briefly, cells were cultured in Slideflasks (Nunc, PolyLabo, Strasbourg, France) during 3 days, followed by incubation with TPC or the different peptide-conjugated TPCs (5 μM) during 3 h. After washing, fluorescence microscopy was performed with an upright epifluorescence microscope (AX70 Provis, Olympus, Rungis, France), equipped with a 100 W mercury vapor lamp, using a filter set consisting of a 400–440 nm band pass excitation filter, associated with a 570 nm dichroic mirror and a 590-nm-long pass filter. Neutral density filters were used in order to reduce photobleaching phenomenon. Fluorescence images were recorded using a ×40 objective during a strictly controlled integration time. The same conditions (light intensity, objective, and integration time) were used for all photosensitizers, to allow comparison.

2.11. Preparation of samples for MALDI-TOF mass spectrometry analyses

Stock solutions in dimethylsulfoxide (2 mM) were used. The photosensitizers were diluted in polyethylene glycol (PEG) 400/ethanol/water (30:20:50, v/v/v) to the concentration required for intravenous (i.v) injection to mice (200 μL/25 g body weight). Female athymic Foxn1 nude mice (*nu/nu*) were used for this study (Harlan, Gannat, France). Animal care and studies were performed according to the European convention for the protection of Vertebrate Animals used for Experimental and other Scientific Purposes, EU directives and The Law on Statute on Animal Experiments in France. Mice (6–7/cage) were maintained in standard cages in isolators. Animals were housed with 12-h light/dark cycle at 22–24 °C and 50% humidity, and they were administered with food and water *ad libitum*. They were anesthetized using an intraperitoneal injection of a mixture of ketamine (Ketalar®, Panpharma, Fougères, France) and xylazine (Rompun®, Bayer Pharma, Puteaux, France) at a dose of 60 mg/kg and 8 mg/kg, respectively. Extraction of the conjugates from plasma was carried out as previously described [10]. The procedure involved solvent precipitation using methanol combined with dimethyl sulfoxide (5/0.1, v/v). Using the response surface methodology, an optimal PDT condition was previously selected to model effects and interactions of photosensitizer dose and light dose in nude mice [6]. In order to explore the stability of the conjugates, we used the optimized photosensitizer dose 2.80 mg/kg (1.75 μmol/kg) for each conjugated photosensitizer injected to the mice *via* the tail vein.

2.12. Statistical analysis

Unless otherwise indicated, all the data are mean values ± s.d. calculated from at least three independent experiments. Mann–Whitney *U* test was used to test for the significant level between independent variables. The level of significance was set to $p < 0.05$.

3. Results

3.1. Chemical structure and photophysical characteristics

ATWLPPR, aTWLPPR and Aψ[CH_2NH]TWLPPR and the corresponding conjugated photosensitizers TPC-Ahx-ATWLPPR, TPC-Ahx-aTWLPPR and TPC-Ahx-Aψ[CH_2NH]TWLPPR were obtained with a final purity greater than 95%, as assessed by analytical RP-HPLC. In the case of conjugates, two isomers, corresponding to the reduction of a double bond on either opposing side of the tetrapyrrolic macrocycle could be observed by analytical RP-HPLC. These isomers arise from the asymmetrical character of the molecule. In our study, coupling using solid phase synthesis allowed site-specific conjugation of the chlorin to the amino-terminus of the peptides in a one to one ratio. This site of attachment on the peptides was chosen for simplicity reasons during synthesis and, more importantly, because the arginine at the carboxy-terminus of the peptide has been shown to be essential for activity [18]. A linker (Ahx) was used to attach the peptide to the photosensitizer, in order to ensure relative individualization of the two moieties of the molecule, and thus to preserve the attractive photophysical characteristics of the photosensitizer TPC and the specificity of peptides for receptors. Identities of TPC-Ahx-ATWLPPR, TPC-Ahx-aTWLPPR and TPC-Ahx-Aψ[CH_2NH]TWLPPR were confirmed by MALDI-TOF mass spectrometry (Fig. 1). The absorption spectra of the conjugates were typical of chlorin derivatives, with the Q_I band having the highest molar extinction coefficient among the four Q bands. Conjugation with the different peptides did not induce significant variations in fluorescence and singlet oxygen quantum yields compared to TPC (Fig. 1).

3.2. Molecular affinity of peptides and conjugated photosensitizers

The molecular affinities of the different compounds for NRP-1, NRP-2 and Flt-1 have been estimated using binding tests. As $VEGF_{165}$ binding to its receptors is heparin dependent, the competitive binding experiments were always carried out in the presence of heparin (2 μg/mL). Peptides and conjugated photosensitizers bound to recombinant NRP-1 and NRP-2 chimeric proteins but were devoid of affinity for VEGF receptor type 1 (Flt-1) (Fig. 2A–C). Indeed, ATWLPPR, aTWLPPR and Aψ[CH_2NH]TWLPPR failed to displace the binding of biotinylated $VEGF_{165}$ to Flt-1 (Fig. 2C). Binding of biotinylated $VEGF_{165}$ to NRP-1 was displaced by ATWLPPR, aTWLPPR and Aψ[CH_2NH]TWLPPR in a concentration-dependent manner (IC_{50} = 7, 8 and 9 μM, respectively) and in a comparable manner, binding to NRP-2 was also displaced by ATWLPPR, aTWLPPR and Aψ[CH_2NH]TWLPPR (IC_{50} = 13, 13 and 22 μM, respectively) (Fig. 2D, left column). TPC-Ahx-ATWLPPR,

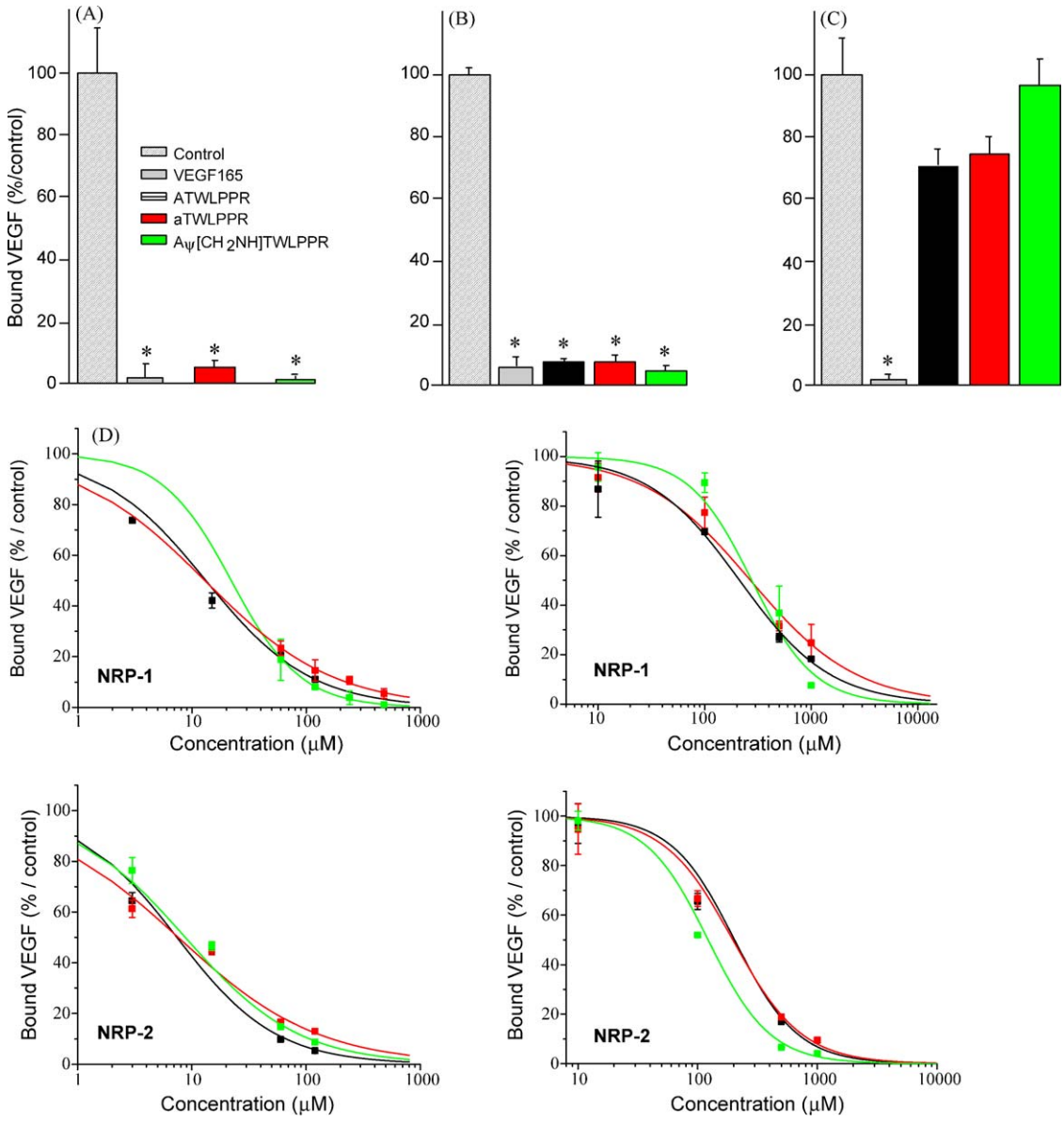

Fig. 2. Binding of peptides and peptides-conjugated TPC to recombinant NRP-1, NRP-2 and Flt-1 proteins (2, 5 and 2 μg/mL, respectively). Biotinylated $VEGF_{165}$ fixation on NRP-1 (A), NRP-2 (B) and Flt-1 (C), without (control) or with $VEGF_{165}$ (0.5, 1.0 and 0.5 μg/mL, respectively), or different peptides (480 μM). Data points show mean ± s.d., $n = 3$. $^*p < 0.05$ *vs.* control. (D) Binding of biotinylated VEGF (5 ng/mL; 110 pM) to NRP-1 and NRP-2 in the presence of 2 μg/mL heparin was evaluated when increasing concentrations of competitors (data points show the mean ± s.d., $n = 3$). Binding of ATWLPPR, aTWLPPR and Aψ[CH_2NH]TWLPPR to NRP-1 and NRP-2 (left column) and corresponding conjugated photosensitizers TPC-Ahx-ATWLPPR, TPC-Ahx-aTWLPPR and TPC-Ahx-Aψ[CH_2NH]TWLPPR (right column).

TPC-Ahx-aTWLPPR and TPC-Ahx-Aψ[CH_2NH]TWLPPR showed affinity for NRP-1 (IC_{50} = 213, 269 and 277 μM, respectively), and NRP-2 (IC_{50} = 203, 197 and 122 μM, respectively) although to a lesser extent than non-conjugated peptides.

3.3. Intracellular uptake of TPC-Ahx-ATWLPPR, TPC-Ahx-aTWLPPR and TPC-Ahx-Aψ[CH_2NH]TWLPPR

For the conjugates TPC-Ahx-ATWLPPR, TPC-Ahx-aTWLPPR and TPC-Ahx-Aψ[CH_2NH]TWLPPR, the intracellular uptake was examined in the dark, at a non-cytotoxic concentration of 5.0 μM. TPC was used as a reference. Fig. 3A shows that the conjugates accumulated up to around 20 times more in NRP-1-expressing wild type MDA-MB-231 (Wt) cells than TPC. Because these enhanced accumulations of the conjugated photosensitizers, compared to TPC, could reflect intracellular uptake but also binding to the membrane without internalization, fluorescence microscopy experiments were undertaken to visualize intracellular uptake. The cells exhibited very intense and diffuse intracellular fluorescence following incubation with TPC-Ahx-ATWLPPR, TPC-Ahx-aTWLPPR and TPC-Ahx-Aψ[CH_2NH]TWLPPR, compared to TPC used at the same concentration (Fig. 3B). This fluorescence emission appeared mainly localized in the cytoplasmic compartment with no detectable nuclear staining.

3.4. NRP-1 knockdown and cellular selectivity

To precise the role of NRP-1 receptor in the cellular uptake of the conjugated photosensitizers, we applied RNA interference (RNAi) technology to knockdown the overexpression of NRP-1 protein in the Wt cells. SiRNA, targeting a sequence of NRP-1 mRNA, was transfected into the Wt cells and the NRP-1 protein level was analyzed by immunoblotting. SiRNA was able to decrease the protein expression of NRP-1 in knockdown MDA-MB-231 cells compared to the parent cells (Wt) and the stably transfected cells with a scrambled siRNA sequence (scrambled) which were used as

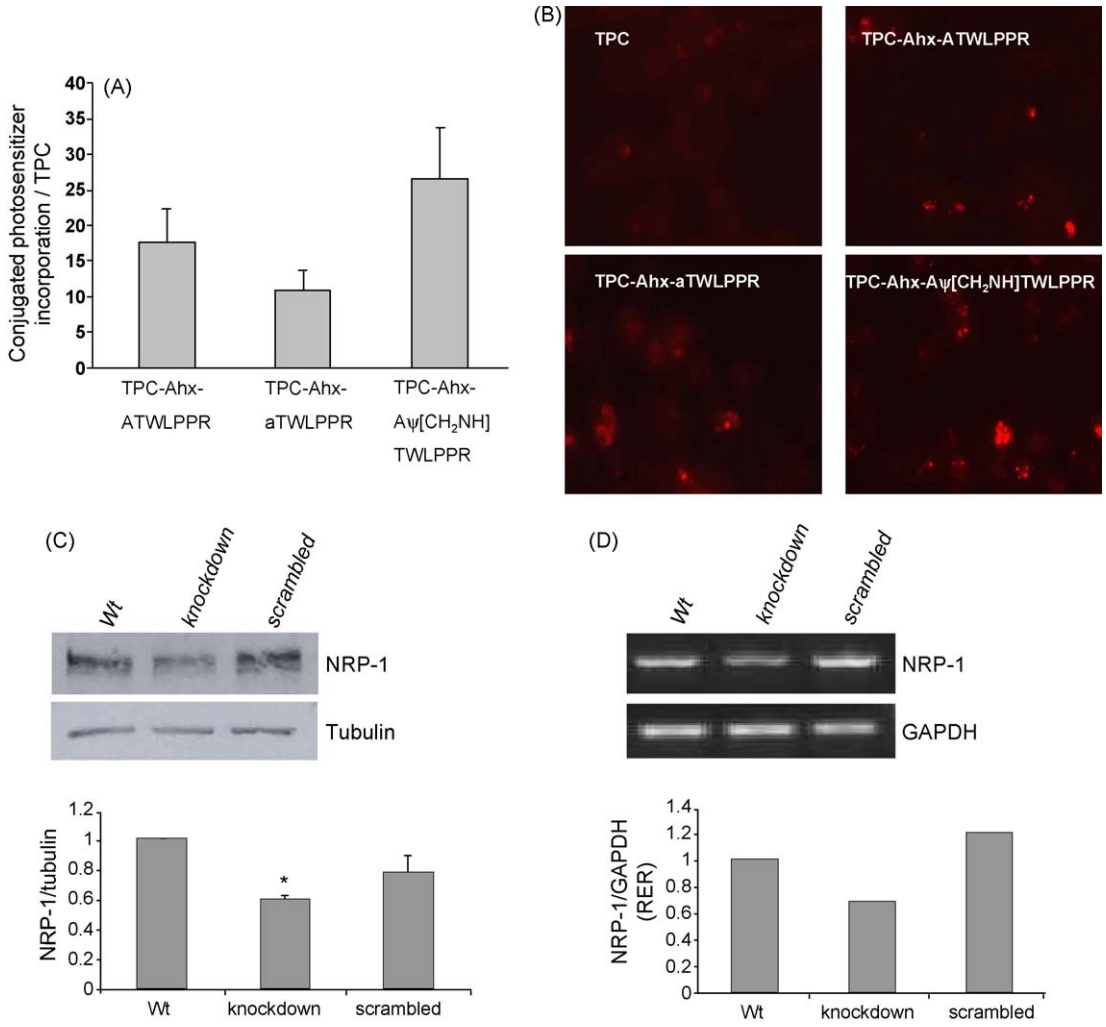

Fig. 3. Relative incorporation rate of peptides-conjugated TPC compared to TPC alone after contact with wild type MDA-MB-231 (Wt) cells for 24 h. The photosensitizer fluorescence intensity was normalized to cell viability. Cells were incubated in the presence of 5 μM photosensitizers. Intracellular fluorescence intensity has been measured at 652 nm after excitation at 415 nm (A). Visualization of cellular uptake by fluorescence microscopy for Wt cells exposed for 3 h to TPC or peptide-conjugated TPC (B). Reduced expression of NRP-1 by siRNA in wild type MDA-MB-231 (Wt) cells, in MDA-MB-231 NRP-1 siRNA (knockdown) cells and in MDA-MB-231 transfected with a scrambled siRNA sequence, (scrambled) cells. Proteins were analyzed in the total protein extracted from cells by Western blot, using either a tubulin or NRP-1-specific polyclonal antibody. Results are representative of three independent experiments (C). Statistically significant difference between Wt and knockdown cells; $^*P < 0.05$. Total RNA was extracted from cells, then subjected to semi-quantitative RT-PCR analysis. The relative levels of NRP-1 mRNA were normalized to those of GAPDH mRNA (D). Data from RT-PCR analysis are expressed as relative expression ratio (RER). Data points show the mean ± s.d. of relative value normalized by report of the chlorin fluorescence, $n = 12$.

control (Fig. 3C). The selected clone exhibited approximately 1.6-fold lower NRP-1 protein expression than the control Wt. No significant difference was observed between MDA-MB-231 Wt cells and MDA-MB-231 cells transfected with the scrambled siRNA (Fig. 3C). The decrease in protein expression was also associated with a decrease in the level of mRNA in NRP-1 siRNA knockdown cells which display a 1.5-fold decrease in NRP-1 relative expression ratio (RER; Fig. 3D).

NRP-1 knockdown leads to decrease in TPC-Ahx-ATWLPPR, TPC-Ahx-aTWLPPR and TPC-Ahx-Aψ[CH_2NH]TWLPPR cellular uptakes (Fig. 4). A statistically significant decrease of different conjugated photosensitizers cellular uptakes after RNA interference-mediated silencing of NRP-1 was evidenced after 2 and 6 h of contact (Fig. 4). The three conjugates displayed a similar uptake rate which increased in function of time.

3.5. In vivo plasma stability

The *in vivo* stability of the peptides-conjugated photosensitizers has been estimated in nude mice plasma at 1 and 4 h post-injection, by mass spectrometry analyses. Four hours after injection, we identified a predominant metabolic product as resulting from the enzymatic cleavage of the peptide bond between the alanyl and threonyl residues of TPC-Ahx-ATWLPPR and TPC-Ahx-aTWLPPR. This main degradation product (TPC-Ahx-A) was detected in plasma from 4 h post-injection. For TPC-Ahx-aTWLPPR, a second degradation site has been also identified into the pseudopeptide moiety between threonine and tryptophan amino acids (Fig. 5). No degradation product of TPC-Ahx-Aψ[CH_2NH]TWLPPR could be observed *in vivo* in plasma up to 4 h after intravenous injection (Fig. 5).

4. Discussion

One of the main disadvantages of peptides is their high sensitivity to proteolysis which could limit their use *in vivo* [8]. In our strategy, peptides are selected as targeting moiety. Indeed, the photodynamic properties of the conjugated photosensitizers are brought by the photosensitizer moiety, while selectivity is due to the presence of the peptide. Thus, a degradation of the peptidic moiety is detrimental to selectivity. The ATWLPPR peptide has already been used in several *in vitro* and *in vivo* studies [19–22],

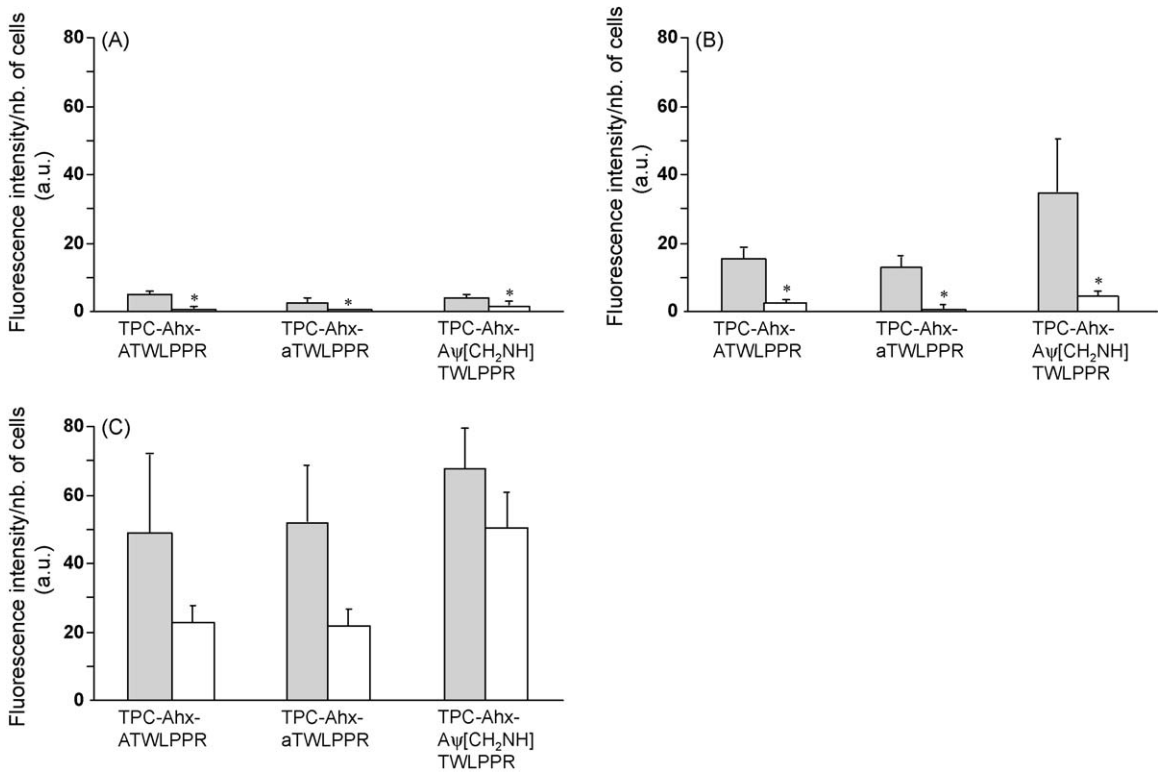

Fig. 4. Uptake of TPC-Ahx-ATWLPPR, TPC-Ahx-aTWLPPR and TPC-Ahx-Aψ[CH_2NH]TWLPPR in Wt cells (grey) compared to knockdown cells (*white*). Cells were incubated with photosensitizers at 5 μM for 2 h (A), 6 h (B) and 24 h (C). Cellular fluorescence intensities after extraction were measured at 652 nm following excitation at 415 nm and cell concentrations were deduced from a calibration curve by MTT test (data points show the mean ± s.d., $n = 12$). $^*P < 0.05$, knockdown *vs.* Wt cells.

but, to the best of our knowledge, none had reported on its instability. We previously investigated the *in vivo* instability of TPC-Ahx-ATWLPPR following i.v. injection into mice; a significant degradation of the peptide was evidenced in plasma from 4 h post injection. This was not really surprising, a variety of proteases are present in human plasma, including both exopeptidases and endopeptidases [23,24]. We have also characterized the main metabolic product as being TPC-Ahx-A [10]. This metabolite has lost any selectivity for angiogenic endothelial cells since the arginyl residue at the C-terminus of the ATWLPPR peptide has been shown to be essential for affinity against NRP-1 [18]. In this study, we evidenced that selection of peptidases-resistant pseudopeptides can improve the peptide stability *in vivo* without loss of its affinity. This approach implied the generation of modified peptides with improved stability properties, through *e.g.* the use of D-amino acids and reduced peptide bonds [8].

For this aim, two optimized pseudopeptides (aTWLPPR and Aψ[CH_2NH]TWLPPR) were studied. We validated the chemical identities of the new conjugated photosensitizers by MALDI-TOF mass spectrometry. Their absorption *spectra* were typical of chlorin derivatives, and the conjugation with the different peptides (ATWLPPR, aTWLPPR or Aψ[CH_2NH]TWLPPR) did not induce significant variations in photophysical properties, fluorescence and singlet oxygen quantum yields.

Affinity for NRP-1 and NRP-2 decreased following coupling to chlorin. Indeed, TPC-Ahx-ATWLPPR, TPC-Ahx-aTWLPPR and TPC-Ahx-Aψ[CH_2NH]TWLPPR showed affinity for both NRPs but to a lesser extent than non-conjugated peptides. Reasons for this may include intramolecular interactions between TPC and peptides, and steric hindrance due to the TPC moiety. The linker was used as a spacer to couple the photoactivable compound to peptides, in order to individualize these two moieties. We previously demonstrated that the conjugation with Ahx alone did not interfere with ATWLPPR binding on NRP-1 [7]. Nevertheless, the presence of a spacer brings flexibility to the molecule, and its length, as well as the nature of the molecule attached to it, may impact on receptor affinity [25,26]. We did not test the influence of varying spacer length on receptors affinity however in another approach, evaluating new peptides targeting NRP-1, some molecular affinity tests were performed with three different spacers (Ahx), polyethylene glycol (PEG)9 (1-amino-3,6-dioxaoctanoic acid), and PEG18 (1-amino-9-aza-3,6,12,15-tetraoxa-10-on-heptadecanoic acid) linked up TPC and new peptides (unpublished results). We evidenced that the spacer length and its nature did not influence the affinity results but led to an increase of solubility with the PEG moieties as linkers. In another previous work, folic acid was conjugated to 4-carboxyphenylporphyrin *via* two short linkers, that were different in nature but similar in size [27]. Both conjugated photosensitizers showed improved intracellular uptake in human oropharyngeal epidermoid carcinoma KB cells, compared to the unconjugated photosensitizer. ATWLPPR has also been shown to bind NRP-2 [21]. Interestingly, new pseudopeptides (aTWLPPR or Aψ[CH_2NH]TWLPPR) exhibited comparable affinities for NRP-1 or NRP-2 compared to the affinity of the reference peptide ATWLPPR.

We evidenced an increase of these conjugates cellular uptake (whatever the conjugated peptide ATWLPPR, aTWLPPR or Aψ[CH_2NH]TWLPPR) compared to chlorin alone and a statistically significant decrease of the conjugated photosensitizers uptake after RNA interference-mediated silencing of NRP-1. Indeed, taking advantage of RNA silencing techniques known as RNAi, we have selectively silenced NRP-1 expression in MDA-MB-231 breast cancer cells to provide the evidence for the involvement of NRP-1 expression in TPC-Ahx-ATWLPPR, TPC-Ahx-aTWLPPR and TPC-Ahx-Aψ[CH_2NH]TWLPPR cellular uptakes. The decrease in NRP-1 protein expression in knockdown MDA-MB-231 cells was associ-

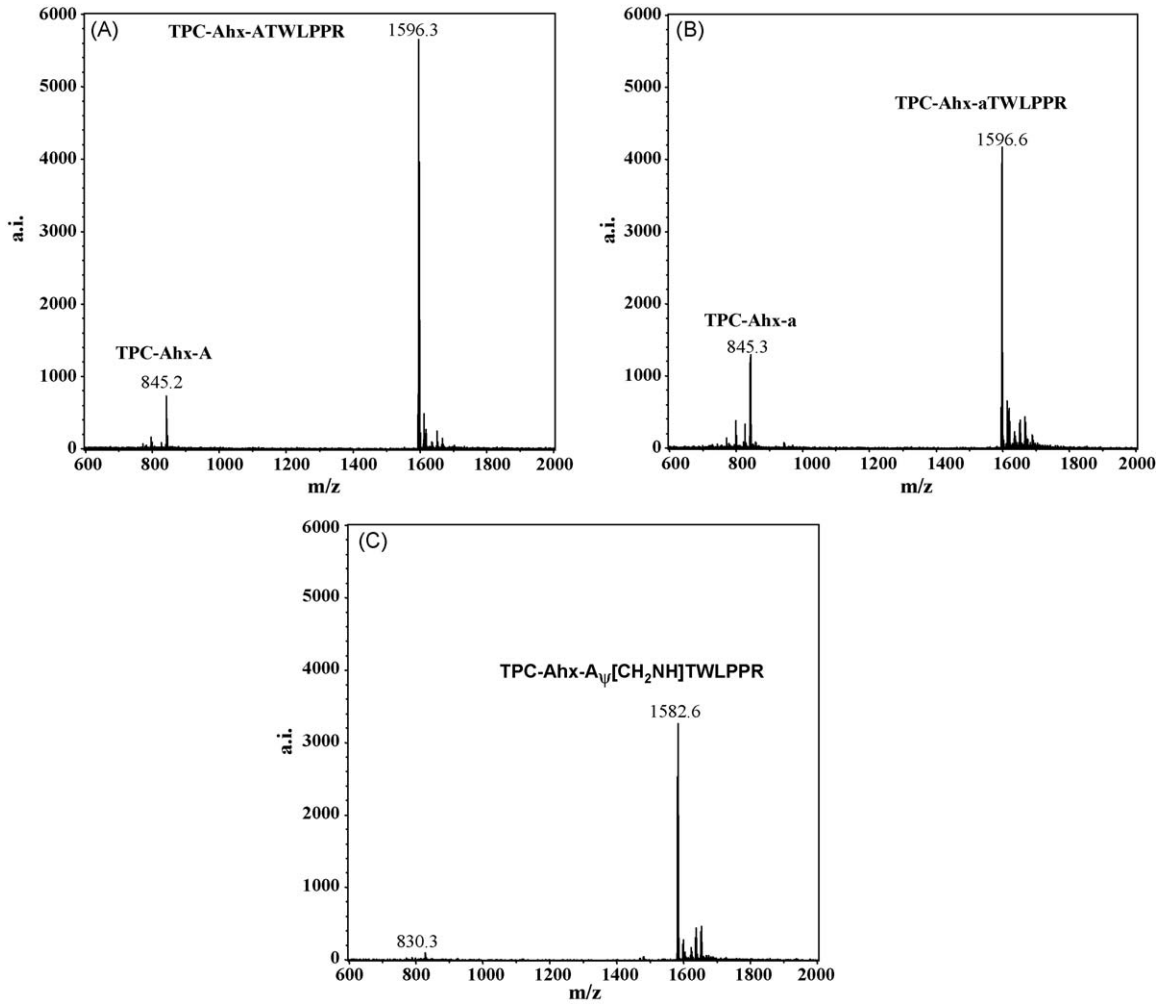

Fig. 5. MALDI-TOF mass spectrum of TPC-Ahx-ATWLPPR (A), TPC-Ahx-aTWLPPR (B) and TPC-Ahx-Aψ[CH_2NH]TWLPPR (C) in nude mice plasma 4 hours after i.v. injection (5.6 mg/mL; 3.5 μmol/kg).

ated with a decrease in the level of transcript. The significant decrease of the conjugated photosensitizers uptake after RNAi-mediated silencing of NRP-1 confirms the involvement of NRP-1 in the conjugates cellular accumulation.

In order to explore the stability of TPC-Ahx-ATWLPPR, TPC-Ahx-aTWLPPR and TPC-Ahx-Aψ[CH_2NH]TWLPPR *in vivo*, conjugates stability were determined in plasma at different times following i.v. injection into mice. As observed for TPC-Ahx-ATWLPPR, the pseudopeptides-conjugated photosensitizers were stable in plasma for at least 1 hour. Whereas TPC-Ahx-ATWLPPR and TPC-Ahx-aTWLPPR were degraded 4 h post-injection, no degradation was observed in plasma for TPC-Ahx-Aψ[CH_2NH]TWLPPR. This result provides essential information for the choice of Aψ[CH_2NH]TWLPPR as an interesting candidate to improve the *in vivo* stability of conjugated photosensitizers.

The present study draws attention to this potential problem using peptides, especially in the case of targeting strategies and these promising results lead us to suggest for instance, the elaboration of multifunctional nanoparticles functionalized by these pseudopeptides for the photosensitizers delivery.

Acknowledgements

This work was supported by the research funds of the French Ligue Nationale Contre le Cancer and the ANR project no. ANR-08-PCVI-0021-01"Nano-VTP".

References

[1] Sharman WM, van Lier JE, Allen CM. Targeted photodynamic therapy via receptor mediated delivery systems. Adv Drug Deliv Rev 2004;56:53–76.
[2] Schneider R, Tirand L, Frochot C, Vanderesse R, Thomas N, Gravier J, et al. Recent improvements in the use of synthetic peptides for a selective photodynamic therapy. Anticancer Agents Med Chem 2006;6:469–88.
[3] Dougherty TJ, Gomer CJ, Henderson BW, Jori G, Kessel D, Korbelik M, et al. Photodynamic therapy. J Natl Cancer Inst 1998;90:889–905.
[4] Folkman J. Angiogenesis in cancer, vascular, rheumatoid and other disease. Nat Med 1995;1:27–31.
[5] Ichikawa K, Hikita T, Maeda N, Yonezawa S, Takeuchi Y, Asai T, et al. Anti-angiogenic photodynamic therapy (PDT) by using long-circulating liposomes modified with peptide specific to angiogenic vessels. Biochim Biophys Acta 2005;1669:69–74.
[6] Tirand L, Bastogne T, Bechet D, Linder M, Thomas N, Frochot C, et al. Response surface methodology: an extensive potential to optimize in vivo photodynamic therapy conditions. Int J Radiat Oncol Biol Phys 2009;75:244–52.
[7] Tirand L, Frochot C, Vanderesse R, Thomas N, Trinquet E, Pinel S, et al. A peptide competing with VEGF165 binding on neuropilin-1 mediates targeting of a chlorin-type photosensitizer and potentiates its photodynamic activity in human endothelial cells. J Control Release 2006;111:153–64.
[8] Adessi C, Soto C. Converting a peptide into a drug: strategies to improve stability and bioavailability. Curr Med Chem 2002;9:963–78.
[9] Thomas N, Tirand L, Chatelut E, Plenat F, Frochot C, Dodeller M, et al. Tissue distribution and pharmacokinetics of an ATWLPPR-conjugated chlorin-type photosensitizer targeting neuropilin-1 in glioma-bearing nude mice. Photochem Photobiol Sci 2008;7:433–41.
[10] Tirand L, Thomas N, Dodeller M, Dumas D, Frochot C, Maunit B, et al. Metabolic profile of a peptide-conjugated chlorin-type photosensitizer targeting neuropilin-1: an in vivo and in vitro study. Drug Metab Dispos 2007;35:806–13.
[11] Coy DH, Heinz-Erian P, Jiang NY, Sasaki Y, Taylor J, Moreau JP, et al. Probing peptide backbone function in bombesin. A reduced peptide bond analogue

with potent and specific receptor antagonist activity. J Biol Chem 1988; 263:5056–60.
[12] Martinez J, Bali JP, Rodriguez M, Castro B, Magous R, Laur J, et al. Synthesis and biological activities of some pseudo-peptide analogues of tetragastrin: the importance of the peptide backbone. J Med Chem 1985;28:1874–9.
[13] Szelke M, Leckie B, Hallett A, Jones DM, Sueiras J, Atrash B, et al. Potent new inhibitors of human renin. Nature 1982;299:555–7.
[14] Neimark J, Briand JP. Development of a fully automated multichannel peptide synthesizer with integrated TFA cleavage capability. Pept Res 1993;6:219–28.
[15] Douat C, Heitz A, Martinez J, Fehrentz JA. Synthesis of N-protected alpha-amino aldehydes from their morpholine amide derivatives. Tetrahedron Lett 2000;41:37–40.
[16] Di Stasio B, Frochot C, Dumas D, Even P, Zwier J, Muller A, et al. The 2-aminoglucosamide motif improves cellular uptake and photodynamic activity of tetraphenylporphyrin. Eur J Med Chem 2005.
[17] Kattan Z, Marchal S, Brunner E, Ramacci C, Leroux A, Merlin JL, et al. Damaged DNA binding protein 2 plays a role in breast cancer cell growth. PLoS One 2008;3:e2002.
[18] Starzec A, Ladam P, Vassy R, Badache S, Bouchemal N, Navaza A, et al. Structure-function analysis of the antiangiogenic ATWLPPR peptide inhibiting VEGF(165) binding to neuropilin-1 and molecular dynamics simulations of the ATWLPPR/neuropilin-1 complex. Peptides 2007;28:2397–402.
[19] Janssen AP, Schiffelers RM, ten Hagen TL, Koning GA, Schraa AJ, Kok RJ, et al. Peptide-targeted PEG-liposomes in anti-angiogenic therapy. Int J Pharm 2003;254:55–8.
[20] Rodrigues S, Van Aken E, Van Bocxlaer S, Attoub S, Nguyen QD, Bruyneel E, et al. Trefoil peptides as proangiogenic factors in vivo and in vitro: implication of cyclooxygenase-2 and EGF receptor signaling. Faseb J 2003;17:7–16.
[21] Perret GY, Starzec A, Hauet N, Vergote J, Le Pecheur M, Vassy R, et al. In vitro evaluation and biodistribution of a 99mTc-labeled anti-VEGF peptide targeting neuropilin-1. Nucl Med Biol 2004;31:575–81.
[22] Renno RZ, Terada Y, Haddadin MJ, Michaud NA, Gragoudas ES, Miller JW. Selective photodynamic therapy by targeted verteporfin delivery to experimental choroidal neovascularization mediated by a homing peptide to vascular endothelial growth factor receptor-2. Arch Ophthalmol 2004;122:1002–11.
[23] McDonald JK, Barrette AJ. Mammalian Proteases: A Glossary and Bibliography. 1. Endopeptidases. London: Academic Press; 1980.
[24] McDonald JK, Barrette AJ. Mammalian Proteases: A Glossary and Bibliography. 2. Exopeptidases. London: Academic Press; 1986.
[25] Kostenich G, Livnah N, Bonasera TA, Yechezkel T, Salitra Y, Litman P, et al. Targeting small-cell lung cancer with novel fluorescent analogs of somatostatin. Lung Cancer 2005;50:319–28.
[26] Engel A, Chatterjee SK, Al-Arifi A, Nuhn P. Influence of spacer length on the agglutination of glycolipid-incorporated liposomes by ConA as model membrane. J Pharm Sci 2003;92:2229–35.
[27] Schneider R, Schmitt F, Frochot C, Fort Y, Lourette N, Guillemin F, et al. Design, synthesis, and biological evaluation of folic acid targeted tetraphenylporphyrin as novel photosensitizers for selective photodynamic therapy. Bioorg Med Chem 2005;13:2799–808.